

RESEARCH ARTICLE

EGFR activation attenuates the mechanical threshold for integrin tension and focal adhesion formation

Tejeshwar C. Rao¹, Victor Pui-Yan Ma², Aaron Blanchard³, Tara M. Urner¹, Shreya Grandhi¹, Khalid Salaita^{2,3} and Alexa L. Mattheyses^{1,*}

ABSTRACT

Mechanical forces, growth factors and the extracellular matrix all play crucial roles in cell adhesion. To understand how epidermal growth factor receptor (EGFR) impacts the mechanics of adhesion, we employed tension gauge tether (TGT) probes displaying the integrin ligand cRGDfK and quantified integrin tension. EGF exposure significantly increased spread area, cell circularity, integrated integrin tension, mechanical rupture density, radial organization and size of focal adhesions in Cos-7 cells on TGT surfaces. These findings suggest that EGFR regulates integrin tension and the spatial organization of focal adhesions. Additionally, we found that the mechanical tension threshold for outside-in integrin activation is tunable by EGFR. Parallel genetic and pharmacologic strategies demonstrated that these phenotypes are driven by ligand-dependent EGFR signaling. Our results establish a novel mechanism whereby EGFR regulates integrin activation and cell adhesion, providing control over cellular responses to the environment.

This article has an associated First Person interview with the first author of the paper.

KEY WORDS: Integrin, Force probes, Mechanotransduction

INTRODUCTION

Mechanical forces are crucial for many cellular functions, including adhesion, migration and proliferation. Mis-regulation of these forces can lead to malignant transformations (Moendarbary and Harris, 2014). Cells attach to the extracellular matrix (ECM) via focal adhesions (FAs), which are integrin-based bidirectional checkpoints that receive information from both outside and inside the cell (Wozniak et al., 2004). Many processes impacted by integrin mechanotransduction are also influenced by receptor tyrosine kinases (RTKs) such as epidermal growth factor receptor (EGFR) (Regad, 2015). Different physical and functional partnerships between a cell, growth factors and the structure and rigidity of the surrounding matrix work together to determine cell fate. Although studies have revealed an interplay between EGFR and integrins, the observed outcomes have been attributed to molecules downstream from the receptors, away from the plasma membrane (Chiasson-MacKenzie and McClatchey, 2018; Dan et al., 2012;

Giancotti and Tarone, 2003; Ricono et al., 2009; Schwartz and Ginsberg, 2002; Vasudevan and Soriano, 2016). Here, we investigate the direct role of EGFR in integrin activation and tension generation during cell attachment and spreading on substrates of varying tension tolerances (Huvneers and Danen, 2009; Saxena et al., 2017; Streuli and Akhtar, 2009). By using tension gauge tether (TGT) surfaces to quantify the amount and location of integrin tension, we have identified a novel function of activated EGFR in mechanically regulating integrin tension and FA formation via its kinase domain. We determined that EGFR–integrin crosstalk attenuates the threshold for outside-in mechanical activation of integrins in a tunable manner, enhancing FA maturation and cellular organization while promoting cell spreading.

RESULTS


EGF modulates cell spreading, integrin tension and FA organization

Evidence suggests that EGFR signaling alters the constituents of FAs, which could have consequences for regulating the mechanical functions of a cell (Eberwein et al., 2015; Xie et al., 1998). The EGFR signaling pathway is activated by epidermal growth factor (EGF), which is a high-affinity ligand for EGFR. Therefore, we first tested whether EGF stimulation impacts cell mechanics. We chose the Cos-7 cell line for this study because it primarily expresses EGFR (ErbB1) over other ErbB isoforms (Fig. S1A). As a mechanical sensing platform, we synthesized surfaces using the ‘turn-on’ TGT probes presenting the integrin ligand cyclic Arg-Gly-Asp-Phe-Lys (cRGDfK) (Fig. S1B) (Liu et al., 2016; Ma et al., 2016; Wang and Ha, 2013). This ligand is highly selective for binding to the $\alpha_v\beta_3$ and, to a lesser extent, $\alpha_v\beta_5$ integrin heterodimers (Kantlehner et al., 2000; Kapp et al., 2017; Kok et al., 2002). TGT probes consist of a DNA duplex conjugated to the coverslip surface by one strand and presenting the ligand on the other. These probes depend on irreversible force-dependent dissociation of the DNA duplex to generate a fluorescent signal that is indicative of cell adhesion forces. The probes rupture at a threshold tension (tension tolerance, T_{tol}) defined as the force required to mechanically ‘melt’ the duplex within 2 s (Fig. 1A). When an integrin binds the cRGDfK ligand and applies a tension larger than T_{tol} the duplex ruptures and generates a permanent ‘turn-on’ fluorescent signal. Any probes that have not been ruptured remain quenched (Fig. 1B).

Previous work showed that cells have poor adhesion on TGTs with $T_{\text{tol}} \leq 33$ pN and significant adhesion on TGTs with $T_{\text{tol}} \geq 43$ pN (Wang and Ha, 2013). This established a tension threshold for integrin activation and cell adhesion that has been considered universal across cell lines (Chowdhury et al., 2015; Wang and Ha, 2013; Wang et al., 2016, 2015). Therefore, we employed TGTs that are chemically identical but with different geometries to cover a broad range of tensions using the ‘unzipping’ ($T_{\text{tol}} = 12$ pN, lower

¹Department of Cell, Developmental, and Integrative Biology, University of Alabama at Birmingham, Birmingham, AL 35294, USA. ²Department of Chemistry, Emory University, Atlanta, GA 30322, USA. ³Wallace H. Coulter Department of Biomedical Engineering, Georgia Institute of Technology and Emory University, Atlanta, GA 30322, USA.

*Author for correspondence (mattheyses@uab.edu)

 T.C.R., 0000-0002-3285-1630; A.L.M., 0000-0002-5119-7750

Handling Editor: Andrew Ewald

Received 7 September 2019; Accepted 4 June 2020

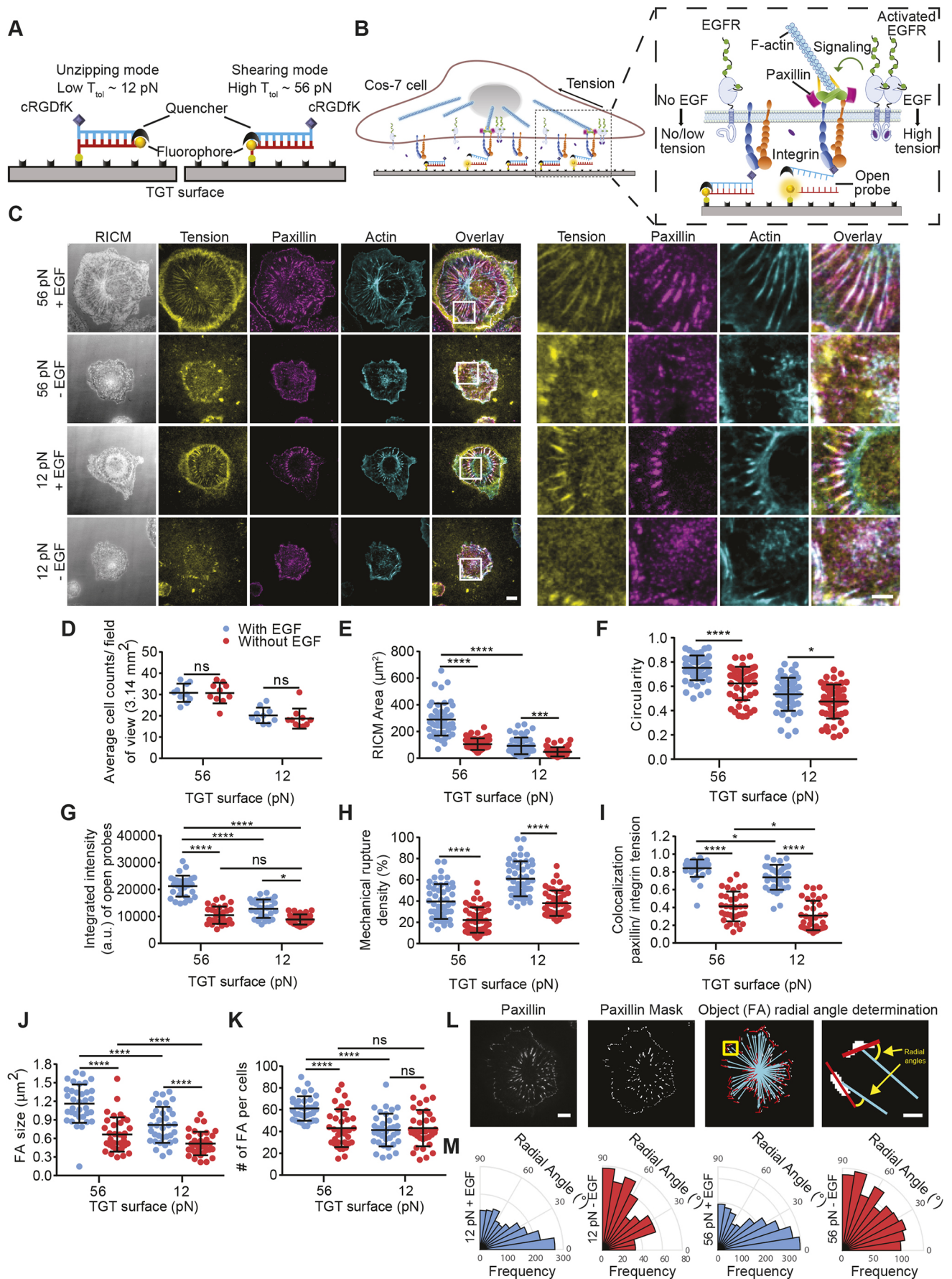


Fig. 1. See next page for legend.

Fig. 1. EGF regulates cell spreading, integrin tension generation and focal adhesion maturation and organization. (A) Schematic of the unzipping (12 pN) and shearing (56 pN) TGT probes. (B) Illustration of the cell–TGT surface contact zone. Inset highlights the interaction of integrins with cRGDfK in the presence (right) or absence (left) of EGF. (C) Images of Cos-7 cells on 56 and 12 pN TGT surfaces 1 h after plating in the presence or absence of EGF with integrin tension (yellow), paxillin (magenta) and actin (cyan). Region of interest (ROI) highlights the subcellular organization and colocalization of integrin tension, paxillin and actin. (D) Scatter plots for the average cell count per field of view (per 3.14 mm²) with or without EGF on both the TGT surfaces ($n=10$ fields of view over three independent experiments). (E–H) Scatter plots for the cell footprint: RICM spread area (E), cell circularity (F), integrated intensity of open probes (G) and the mechanical rupture density (H) for Cos-7 cells with or without EGF stimulation. (I) Colocalization of paxillin and integrin tension was assessed by Pearson's correlation coefficient ($n=50$ cells, three independent experiments). (J,K) Scatter plots for FA size (J) and the number of FAs per cell (K) for Cos-7 cells with or without EGF stimulation ($n=50$ cells, three independent experiments). (L) Representative example for a paxillin mask generated using the paxillin image and the cell mask boundary (not shown). A centripetal axis (blue), from the cell centroid to the FA centroid, was obtained for each FA. The angle between the long axis and the centripetal axis represents the radial angle of each object. (M) Rose plots showing the radial distribution of FA orientations (12 pN TGT, $n=35$ cells with EGF, $n=29$ cells without EGF; 56 pN TGT, $n=28$ cells with EGF, $n=44$ cells without EGF; three independent experiments). Bars indicate mean \pm s.d. Differences between the groups were assessed statistically with either a Student's *t*-test (D) or one-way ANOVA (E–K); ^{ns} $P>0.05$, * $P<0.05$, *** $P<0.001$, **** $P<0.0001$. Scale bars: 10 μ m, ROI scale bar 5 μ m (C); 10 μ m, ROI scale bar 1.5 μ m (L).

tension threshold) and 'shearing' ($T_{\text{tot}}=56$ pN, higher tension threshold) modes (Fig. 1A) (Mosayebi et al., 2015; Wang and Ha, 2013; Wang et al., 2015). Importantly, T_{tot} affects only the mechanosensation properties of the cells, due to differing probe geometries, whereas the integrin–ligand interaction remains unchanged (Wang et al., 2018b; Zhang et al., 2018). The mechanically ruptured 'turn-on' TGT probes report the history of integrin tension over the course of the experiment. Imaging by high-resolution fluorescence microscopy allows us to quantify the amount and spatial distribution of integrin tension (Fig. 1C).

First, we asked whether EGF stimulation had an impact on the overall attachment of cells to the TGT surfaces. There was no significant difference in the total number of cells attached to the surfaces 1 h after plating, with or without EGF (Fig. 1D). However, the number of cells that adhered was dependent on the tension threshold. More cells attached on the higher threshold 56 pN TGT surface, in agreement with previous studies (Wang and Ha, 2013). Next, we investigated the effects of EGF stimulation on cell adhesion and spreading in terms of changes in cell morphology, cell mechanics and FAs. For this analysis, cells were fixed 1 h after plating and imaged with reflective interference contrast microscopy (RICM) and total internal reflection fluorescence (TIRF) microscopy (Fig. 1C). RICM images reveal the cell–substrate contact region, also known as the cell footprint area, which reports the ability of a cell to spread on the surface. TIRF microscopy illuminates a ~ 100 nm region adjacent to the coverslip, highlighting cell–TGT interactions and cell membrane-associated proteins while eliminating any other fluorescent signals from deeper within the cell. We observed interesting changes in cell morphology, including changes in cell shape, larger cell footprints, increased tension and enhanced organization of FAs and actin with EGF stimulation.

Cell spreading, quantified by the area of the cell footprint, was enhanced on the 56 pN surface compared with the 12 pN surface (Fig. 1E). This was expected as it has previously been shown that cell adhesion is reduced when integrin tension generation is restricted on substrates with lower tension thresholds (Wang and Ha, 2013). We also found that EGF stimulation caused cells to spread more on both

the 56 pN and 12 pN TGT surfaces. The ability of EGF to enhance spreading on the 12 pN TGT surface was unexpected and suggests that EGF can lower the threshold of cell-generated tension required for spreading. Morphology was quantified by determining the circularity of the cell footprint, with values closer to 1 representing a more circular cell. Cells adopted a more circular morphology when stimulated with EGF on both TGT surfaces (Fig. 1F).

We next wanted to know whether these morphological changes corresponded to changes in cell mechanics. First, we quantified the integrated integrin tension as the total fluorescence of open TGT probes within the RICM footprint. The integrated tension represents all the events where tension above T_{tot} was generated on an integrin engaged with its cognate ligand at some time during the experiment. EGF stimulation led to a significant increase in integrated integrin tension on both the 'higher' and 'lower' threshold TGT surfaces (Fig. 1G). Next, we quantified the mechanical rupture density to investigate the mechanical exploration of the cell contact region. The mechanical rupture density is the percentage of the cell contact area that experienced mechanical tension higher than T_{tot} over the course of the experiment. This metric is dependent on the cell spread area being maximum at the time of measurement. On both TGT surfaces, the mechanical rupture density was significantly higher with EGF stimulation (Fig. 1H). This indicates that EGF stimulation increased the cell area with integrin forces as well as the total number of ruptured probes. The mechanical rupture density was higher on the 12 pN TGT surface than on the 56 pN TGT surface, indicating that more of the contact region was subjected to forces large enough to rupture the probe (Fig. 1F–H). This data further shows that the tension threshold of the underlying TGT surface had a larger effect than EGF stimulation on the probability of probe rupture. When interpreting these results it is important to consider that different combinations of cellular forces can produce similar fluorescence outcomes (Murad and Li, 2019; Yasunaga et al., 2019). We could not discern whether differences in integrated tension or mechanical rupture density were due to a change in the number of individual receptors generating forces or the frequency of individual receptor–ligand interactions, only that there was an increase in the number of open probes and a change in their distribution.

To verify that cell attachment to the TGT surface was mediated through integrin–ligand interactions, cells were plated on control surfaces containing TGT probes not conjugated to cRGDfK. Cells plated on the control surfaces did not adhere and there was no measurable tension, demonstrating the specificity of the cRGDfK–integrin interaction in our readout (Fig. S1C). Additionally, we verified the specificity of the $\alpha_v\beta_3$ and $\alpha_v\beta_5$ integrins in the observed cellular responses using the inhibitor SB273005 (K_i of 1.2 nM and 0.3 nM for $\alpha_v\beta_3$ and $\alpha_v\beta_5$, respectively) (Duong and Coleman, 2002). Treatment with SB273005 in the presence of EGF resulted in a reduction in both cell spread area and integrated integrin tension to levels not statistically different from those in untreated cells without EGF stimulation (Fig. S2). This shows that the observed cellular responses on the cRGDfK TGT surfaces were mediated through the interaction of $\alpha_v\beta_3$ and $\alpha_v\beta_5$ integrin heterodimers with the cRGDfK ligand.

To confirm that the tension signal was generated at FAs, we measured the colocalization of paxillin (an FA protein) and integrin tension using Pearson's correlation coefficient. We found that colocalization was higher following EGF stimulation on both TGT surfaces (Fig. 1I). This suggests that EGFR regulates FA protein recruitment and localization to sites of contact formation following integrin–cRGDfK engagement. These results are in accordance with previous work showing that integrin forces overlap with FA

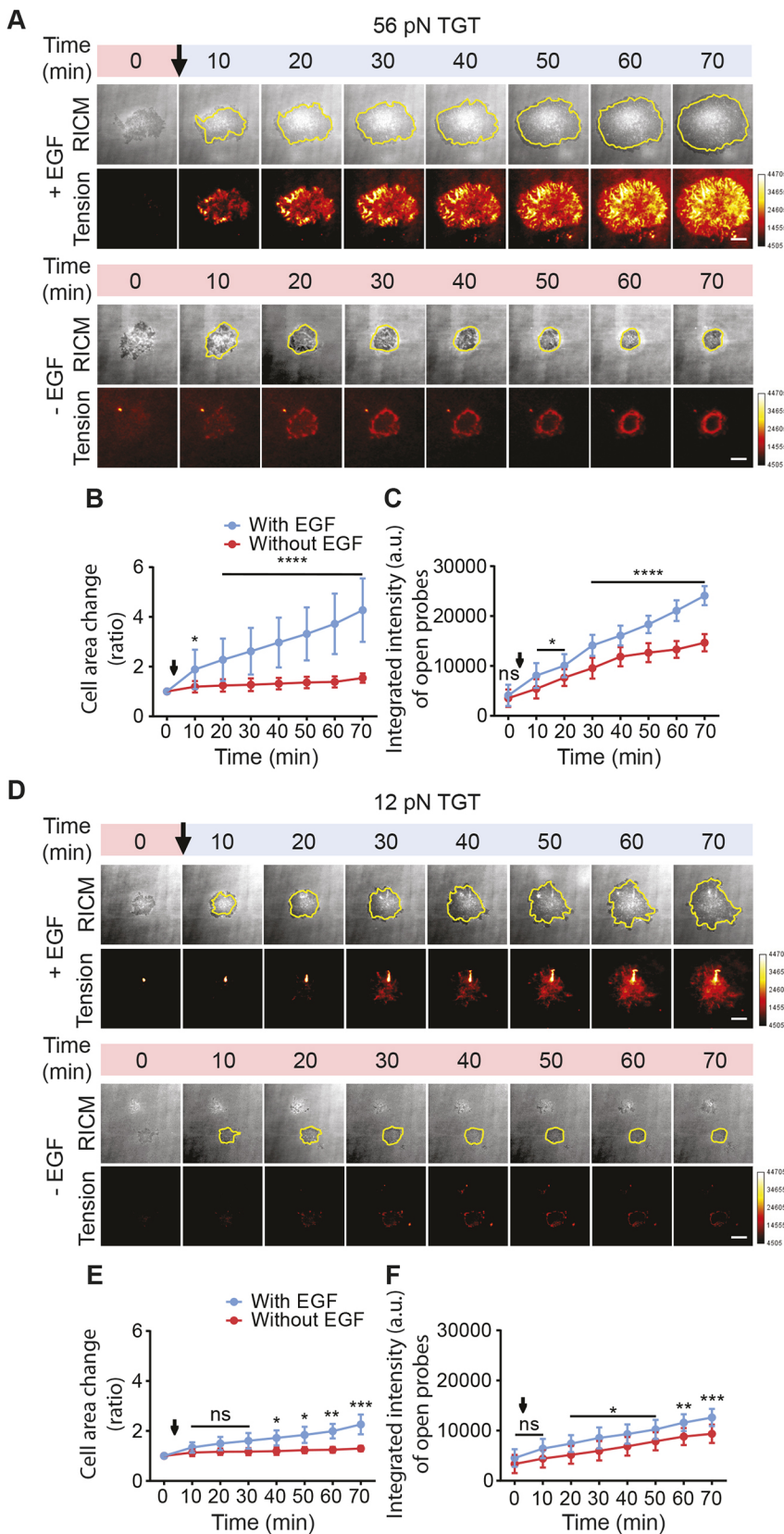


Fig. 2. EGF stimulation causes dynamic changes in cell spreading and integrin tension. (A) RICM and integrated integrin tension for Cos-7 cells plated on 56 pN TGT surfaces in the presence or absence of EGF. Yellow outline shows cell border at previous time point. Arrow indicates addition of EGF. (B,C) Plots showing the average relative change in cell area (B) and integrated tension of open probes (C) with or without EGF stimulation on the 56 pN TGT surface over time. (D) RICM and integrin tension for Cos-7 cells plated on 12 pN TGT surfaces in the presence or absence of EGF. (E,F) Plots showing the average relative change in cell area (E) and integrated tension of open probes (F) with or without EGF stimulation on the 12 pN TGT surface over time ($n=10$ cells; across three independent experiments). Bars indicate mean \pm s.d. $^{ns}P>0.05$, $^{*}P<0.05$, $^{**}P<0.01$, $^{***}P<0.001$, $^{****}P<0.0001$ (Student's t -test). Scale bars: 10 μ m

centroids (Plotnikov et al., 2012; Wang et al., 2015). Together, the data suggest that EGF increases cell sensitivity to integrin–ligand engagement, encouraging cell spreading even on surfaces with lower tension thresholds.

Given the impact of EGF on cell adhesion and mechanics, we next looked at the underlying subcellular structures, FAs. FAs are poised to be a necessary funnel through which changes in extracellular features, including substrate compliance, ligand

availability or growth factor concentration, are transmitted to regulate cell spreading. Paxillin was used as a marker as it is present throughout FA maturation and development (Gardel et al., 2010). We first quantified FA number and size (ranging from 0.2 to 10 μm^2 ; puncta below 0.2 μm^2 were not included in the analysis) to understand the effect of EGF stimulation on FA formation and maturation. FA size is correlated to maturity, whereby larger FAs ($>1 \mu\text{m}^2$) represent more mature adhesions and smaller FAs ($0.2 \mu\text{m}^2 < \text{FA} < 0.6 \mu\text{m}^2$) represent nascent adhesions (Choi et al., 2008; Gardel et al., 2010). Overall, FAs were smaller and less mature in cells on the 12 pN TGT surface (Fig. 1J). FAs were larger in cells supplemented with EGF compared to those in cells without EGF on both TGT surfaces, underscoring the effect of EGF stimulation on FA maturation (Fig. 1J). Next, we quantified the number of FAs per cell to understand the effect of EGF on FA nucleation. EGF stimulation led to an increase in the number of FAs per cell on the 56 pN but not the 12 pN TGT surface (Fig. 1K). This suggests that FA maturation alone promotes cell spreading on the 12 pN TGT surface, whereas both increased maturation and nucleation play a role for the 56 pN surface.

To quantify their spatial organization, the orientation of individual FAs was defined as the angle between a line from the cell center to the FA centroid and the long axis of the FA, called the radial angle (Fig. 1L; Fig. S3A–D). This analysis revealed that with EGF stimulation FAs were radially organized on both TGT surfaces (Fig. 1M; Fig. S3E–G). Without EGF, FAs were organized parallel to the cell periphery on the 12 pN TGTs or randomly on the 56 pN TGTs, demonstrating that EGF plays a role in the radial organization of FAs. Together, these data show that EGF enhances integrin tension, FA organization and FA maturation, thereby facilitating cell spreading.

Additionally, Cos-7 cells were plated onto glass coverslips coated with fibronectin to control for nuances of the TGT probes (Masuda et al., 2014). For cells on fibronectin, EGF stimulation led to an increase in cell area, similar to that on 56 pN TGT, demonstrating that our results are not due to the TGT probes (Fig. S4). To test whether these findings were generalizable, we used multiple cell lines representing different lineages, sources and phenotypes, including NIH/3T3 (mouse, fibroblast), ATDC5 (mouse, epithelial), OV4 (human, epithelial) and HeLa (human, epithelial) (Fig. S5A). In all cell lines examined, EGF stimulation led to enhanced cell spreading and integrin tension on both TGT surfaces (Fig. S5B–E). Taken together, the data suggest that there is not a single tension threshold for cell adhesion and that EGF signaling serves as a compensatory mechanism able to tune the mechanosensitivity of integrins. This tuning of the force threshold for integrin activation increases the ability of cells to stably adhere and spread on substrates with lower tension thresholds.

EGF is required for FA initiation and maturation but not for maintenance

Next, we examined how the dynamics of cell spreading and integrin tension were impacted by EGF. Cells plated on the 56 pN TGT surface attached and began exerting integrin forces within 10 min. In cells stimulated with EGF, the spread area increased over the course of the experiment (Fig. 2A,B). In contrast, cells without EGF showed diminished spreading, with no significant change in spread area over the imaging period (Fig. 2A,B). Integrated integrin tension steadily increased over the course of the experiment at a faster rate with EGF stimulation (Fig. 2C). Without EGF, the cell footprint remained constant, as cells were unable to establish adhesions to support spreading with tension less than T_{tol} . However, cells

actively engaged the surface and generated tension to open the probes, as indicated by the increasing integrated tension. Cells on the 12 pN surface had the same responses to EGF, but with relatively smaller changes in spread area and integrated tension (Fig. 2D–F). Control experiments that involved the exchange of medium while maintaining the same treatment conditions showed no apparent change in cell area or integrin tension (data not shown).

These experiments showed that the ability of cells to spread was significantly reduced without EGF. To test whether EGF could rescue stalled cell spreading, we imaged cells before and after addition of EGF (Fig. 3A). Although cells initially showed limited spreading, the spread area began to increase following the addition of EGF (Fig. 3C). The kinetics of the changes in cell area before and after EGF stimulation were comparable to control experiments without or with EGF, respectively (Fig. 3C). Similarly, the intensity of open probes was initially limited and began increasing at a faster rate with EGF (Fig. 3D). This showed that EGF promoted cell spreading and modulation of the tension threshold in cells whose adhesion was initiated in the absence of EGF. Next, we tested whether removal of EGF would inhibit cell spreading by imaging cells plated in the presence of EGF for 40 min and then switched to medium without EGF (Fig. 3B). Cell spreading was stalled following the removal of EGF, comparable to the no-EGF control (Fig. 3C). Similarly, the integrated intensity was also stalled, indicating reduced integrin tension with removal of EGF (Fig. 3D). Thus, changes in EGF availability can dynamically tune cell spreading and force generation in individual cells.

To identify the involvement of EGF in FA formation and maturation during the above experiments, cells were plated on 56 pN TGT surfaces, subjected to different EGF stimulation paradigms, fixed at different time points and imaged following staining for paxillin and actin (Fig. S6). The number of FAs was not significantly different when cells were stimulated with EGF for 50 or 90 min, even if those cells were subsequently switched to medium without EGF (Fig. 3E). The number of FAs was lower in cells without EGF stimulation, with no significant difference between cells on the surface for 50 or 90 min. FA size was significantly larger with EGF stimulation. Interestingly, cells exposed to EGF for 90 min had slightly larger FAs than those in EGF for 50 min (Fig. 3F). There was not a significant difference in FA size in cells first treated with EGF for 50 min followed by either fixation or a switch to no EGF for an additional 40 min. This indicates that the time of EGF exposure did not influence the number of FAs but did promote maturation. Removal of EGF did not reverse FA maturation or cell adhesion but rather stalled it. Together, the data demonstrate that EGF promotes cell spreading, integrin tension and FA formation, but is not required for FA maintenance.

Activated EGFR regulates integrin tension and FA maturation via the cytoskeleton

The role of the cytoskeleton in EGF-stimulated integrin tension generation was determined by treating cells with inhibitors to F-actin assembly (latrunculin B) and myosin II ATPase (blebbistatin). Cells stimulated with EGF and treated with blebbistatin or latrunculin B had significantly reduced spread area, integrated tension, and circularity in comparison to the untreated controls on the 56 pN TGT surface (Fig. 4A–D). Although EGF stimulation has been shown to lead to phosphorylation of the myosin regulatory light chain (MRLC), promoting myosin-II contraction concurrent with FA formation (Iwabu et al., 2004; Schneider et al., 2009), our results show that EGF stimulation by itself cannot override the effects of cytoskeletal inhibition on integrin tension generation.

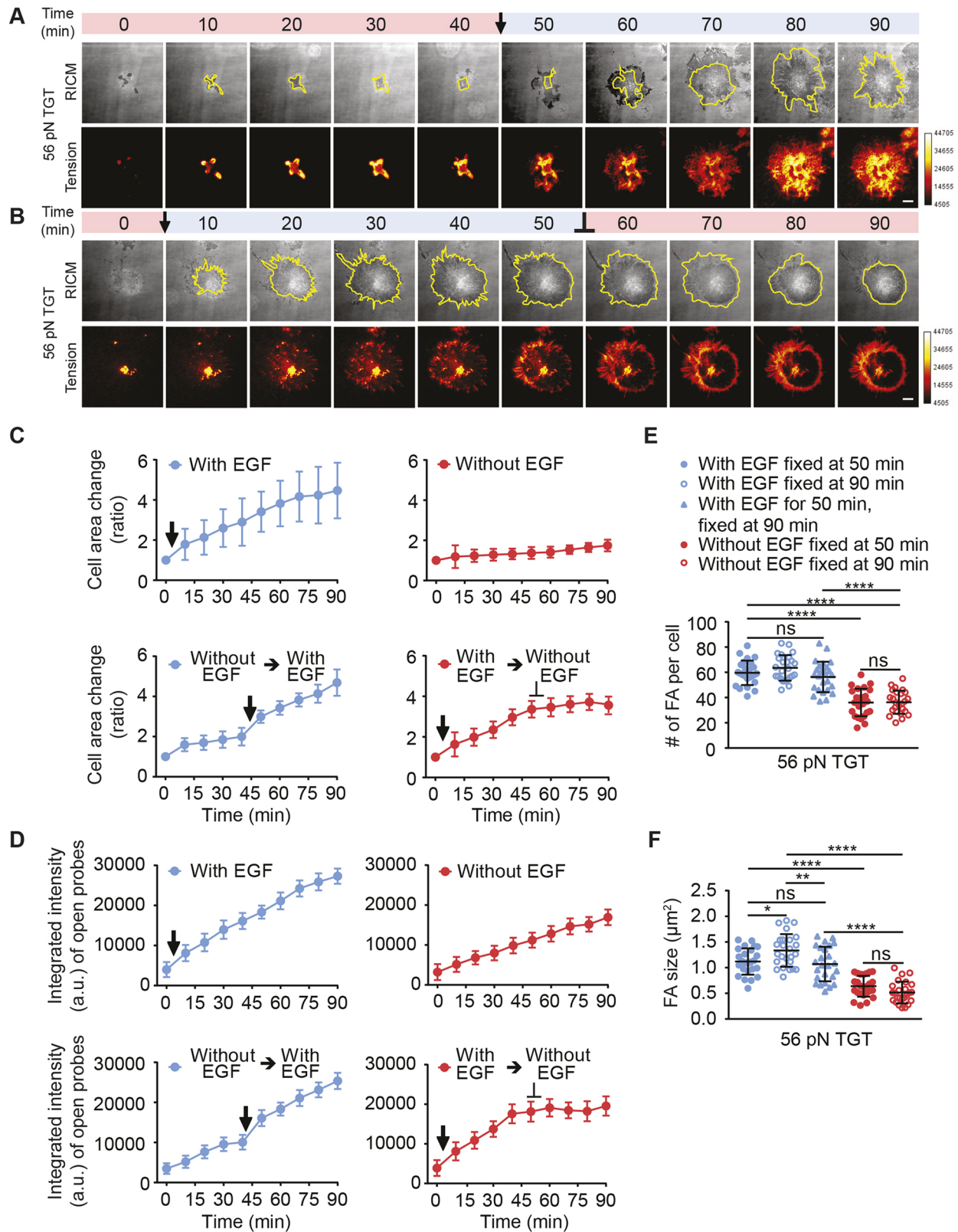


Fig. 3. EGF is essential for focal adhesion initiation and maturation but not maintenance. (A,B) Representative examples for two different ligand treatment paradigms following plating of Cos-7 cells on the 56 pN TGT surface. Paradigm 1 (A): switch from medium without EGF to medium with EGF, indicated by arrow. Paradigm 2 (B): switch from medium with EGF to without EGF, indicated by inverted 'T'. (C,D) Mean cell area change ratio over time (C) and mean integrated intensity of the open probes over time (D) for the indicated control and treatment paradigms ($n=10$ cells across three sets of experiments). (E,F) Scatter plots comparing FA number (E) and FA size (F) ($n=25$ cells across three independent experiments). Bars indicate mean \pm s.d. $^{ns}P>0.05$, $^{*}P<0.05$, $^{**}P<0.01$, $^{****}P<0.0001$ (one-way ANOVA).

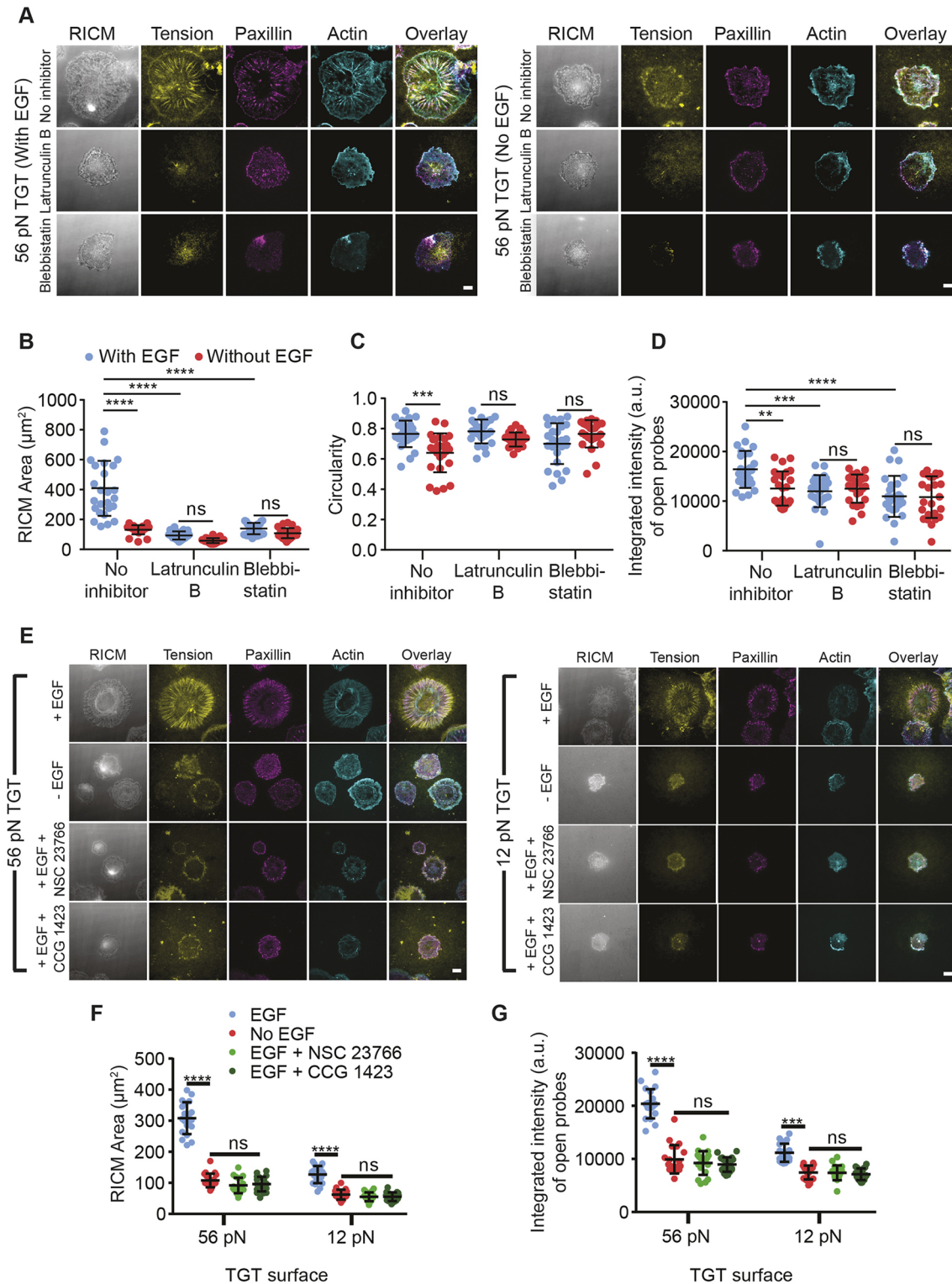


Fig. 4. Acto-myosin pathway inhibition leads to loss of integrin tension and reduced cell spreading. (A) Cos-7 cells treated with control (DMSO alone), latrunculin B or blebbistatin in the presence (left) or absence (right) of EGF on a 56 pN TGT surface fixed and stained 1 h after plating. RICM, integrin tension (yellow), paxillin (magenta) and actin (cyan) are shown. (B–D) Scatter plots for the cell footprint: RICM area (B), cell circularity (C) and the integrated intensity of open probes (D) for Cos-7 cells in each treatment group with or without EGF stimulation ($n=25$ cells across three independent experiments). (E) Cos-7 cells treated with control (DMSO alone), NSC 23766 (Rac1 inhibitor) or CCG 1423 (RhoA inhibitor) in the presence or absence of EGF on both the 56 pN and 12 pN TGT surfaces fixed and stained 1 h after plating. RICM, integrin tension (yellow), paxillin (magenta), and actin (cyan) are shown. (F,G) Scatter plots for the cell footprint: RICM area (F) and the integrated intensity of open probes (G) for Cos-7 cells in each treatment group with or without EGF stimulation ($n=20$ cells across three independent experiments). Bars indicate mean \pm s.d. $^{ns}P>0.05$, $^{*}P<0.01$, $^{***}P<0.001$, $^{****}P<0.0001$ (one-way ANOVA). Scale bars: 10 μm .

EGF signaling has a role in regulating Rho GTPases during cell adhesion, migration, and proliferation in coordination with myosin activity and actin dynamics (Wang et al., 2018a). In addition, EGFR stimulation can promote cytoskeletal reorganization and FA maturation through Rho signaling (Kakiashvili et al., 2011; Paszek et al., 2005; Tong et al., 2016). Therefore, we interrogated the role of RhoA/Rac in regulating EGF-stimulated integrin tension. Cells were treated with inhibitors against RhoA (CCG-1423) and Rac1 (NSC 23766) and plated onto 56 pN TGT surfaces (Fig. 4E) (Evelyn et al., 2007; Levay et al., 2013). Inhibition of RhoA or Rac1 significantly reduced the cell spread area (Fig. 4F) and integrated tension (Fig. 4G) in comparison to untreated controls.

Activated EGFR regulates cell spreading, integrin tension, and FA maturation

To validate the specific role of EGFR in cell adhesion and integrin mechanics, we used the small molecule tyrosine kinase inhibitors Erlotinib and Tyrphostin, which target the EGFR catalytic domain. Both inhibitors reduced EGFR activation in Cos-7 cells as reported by

reduced phosphorylated EGFR staining (Fig. 5A). Inhibitor treatment of Cos-7 cells resulted in a significant reduction of cell spread area, compared to DMSO treated controls (Fig. 5B). Inhibitor treated cells did not acquire the morphology of control cells as indicated by a reduction in cell circularity (Fig. 5C). Additionally, inhibitor treatment of cells stimulated with EGF resulted in a reduction of integrin tension to levels not significantly different from controls without EGF stimulation (Fig. 5D). FAs were observed to be punctate and randomly distributed. We conclude that FAs were arrested in the nascent conformation by EGFR inhibition (Fig. 5E). The data indicate that EGFR kinase signaling plays a crucial role in enhancing integrin tension, cell spreading and FA maturation.

The role of EGFR in regulating integrin tension and FA organization was further validated by siRNA silencing. In Cos-7 cells transfected with EGFR siRNA there was an 80% reduction in EGFR protein level compared with controls transfected with scrambled siRNA (Fig. 6A,B). EGFR silencing resulted in disorganized cytoskeleton and FAs (Fig. 6C), with a significant reduction in the cell spread area (Fig. 6D) and disruption of cell

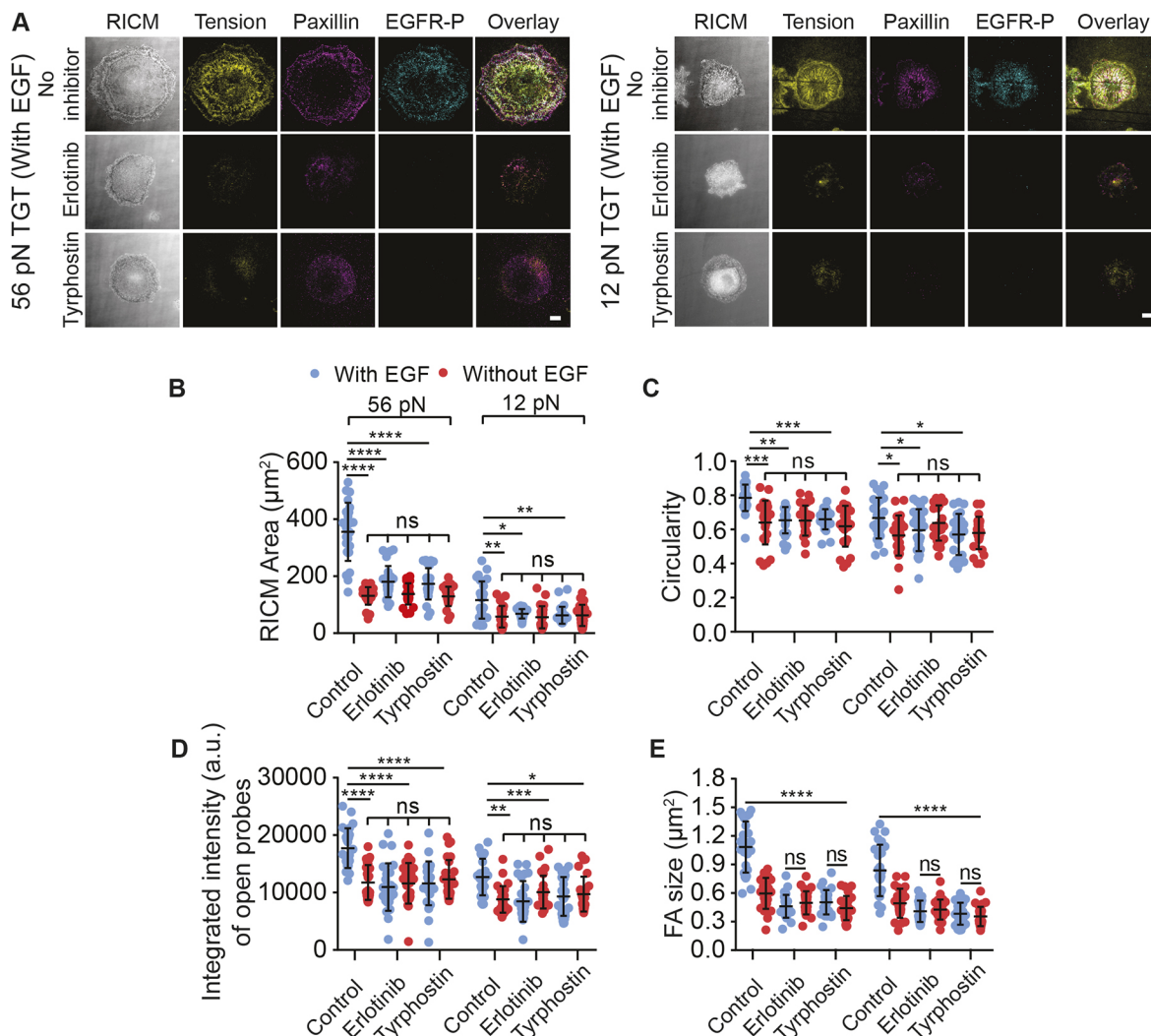


Fig. 5. Tyrosine kinase inhibitors reduce cell spreading, integrin tension and FA maturation. (A) Cos-7 cells treated with control (DMSO alone), Erlotinib HCl or Tyrphostin in the presence of EGF on the 56 pN (left) and 12 pN (right) TGT surfaces 1 h after plating. Shown here are integrin tension (yellow), actin (magenta) and phosphorylated EGFR (cyan). (B–E) Scatter plots for the cell footprint: RICM spread area (B), cell circularity (C), integrated intensity of open probes (D) and FA size (E) for Cos-7 cells in each treatment group with or without EGF stimulation ($n=25$ cells across three independent experiments). Bars indicate mean \pm s.d. $^{ns}P>0.05$, $^{*}P<0.05$, $^{**}P<0.01$, $^{***}P<0.001$, $^{****}P<0.0001$ (one-way ANOVA). Scale bars: 10 μm .

morphology (Fig. 6E). The integrated integrin tension (Fig. 6F) and mechanical rupture density (Fig. 6G) were significantly lower than in scrambled siRNA controls. EGFR-silenced cells had no response to EGF stimulation, as shown by the lack of statistical difference between groups with or without EGF stimulation. In all metrics, the EGFR-silenced cells behaved similarly to control cells without EGF stimulation. These results validate the direct role of EGFR in modulating integrin tension, FA organization and cell spreading.

Activated EGFR regulates cell spreading and integrin force generation via the EGFR autophosphorylation domain

To identify the specific amino acid residues in EGFR responsible for these effects, we generated several EGFP-tagged phosphorylation mutants with altered signaling properties. Upon ligand binding, EGFR dimerizes and undergoes autophosphorylation. Simultaneous autophosphorylation of three principal tyrosine residues (Y1068, Y1148 and Y1173) regulates receptor kinase activity and is necessary for rapid receptor internalization and degradation (Helin and Beguinot, 1991; Sorkin et al., 1992). Additional phosphorylation of two minor sites (Y1086 and Y992) is essential for achieving complete activation (Sorkin et al., 1992). Using site-directed mutagenesis, we mutated either the three principal (triple mutant) or all five (penta mutant) tyrosine residues to phenylalanine (Fig. 7A). Moreover, EGFR, like other RTKs, can be transactivated following integrin engagement (Moro et al., 2002, 1998). This ligand-independent activation occurs via phosphorylation of Y845 by Src kinase. Therefore, we also mutated Y845 (Src mutant) to investigate the role of ligand-independent EGFR activation.

To test the role of EGFR phosphorylation in these processes, we performed rescue experiments in Cos-7 cells treated with EGFR siRNA. First, we used semiquantitative western blotting to validate the expression levels of EGFR and phospho-EGFR following siRNA knockdown and rescue (Fig. 7B). Total EGFR expression levels were comparable to control lysates without knockdown across the different EGFR mutants (Fig. 7D). The levels of EGFR activity were in direct correlation to the degree of tyrosine mutation (Fig. 7C). Transfection with wild-type (WT) EGFR completely rescued the knockdown of EGFR. In cells rescued with WT EGFR, cell morphology, quantified by cell spread area and circularity, and cell mechanics, quantified by integrated tension and mechanical rupture density, were not significantly different from those in control cells (Fig. 7E–I; Tables S1–S4). FAs in these cells were mature and radially organized (Fig. 7E, J–L; Tables S5, S6). Cells transfected with the triple and Src EGFR mutants showed an intermediate phenotype when stimulated with EGF. Cell spread area and integrated tension for these cells ranged between those for WT EGFR with and without EGF stimulation, probably due to the partial loss of EGFR activity in these mutants (~50%, Fig. 7C) (Helin and Beguinot, 1991). Although the changes in cellular responses were similar, they can be attributed to different pathways: altered MAPK/ERK signaling for the triple mutant and the non-canonical STAT pathway in the case of the Src mutant (Helin and Beguinot, 1991; Kloth et al., 2003; Sato et al., 2003). Cells treated with the Src kinase inhibitor PP2 decreased integrated tension and spread area significantly (Fig. S7). However, this may be the result of the combinatorial effects of blocking Src kinases, which inhibit downstream integrin signaling in addition to ligand-independent EGFR signaling. Finally, cells were transfected with the penta mutant, which has a dysfunctional kinase domain and is unable to activate EGFR signaling (Fig. 7C) (Sorkin et al., 1992). The morphology and tension of these cells were not significantly different from WT cells with no EGF stimulation or from EGFR-silenced cells (Fig. 7E–I). FAs in these cells lacked radial

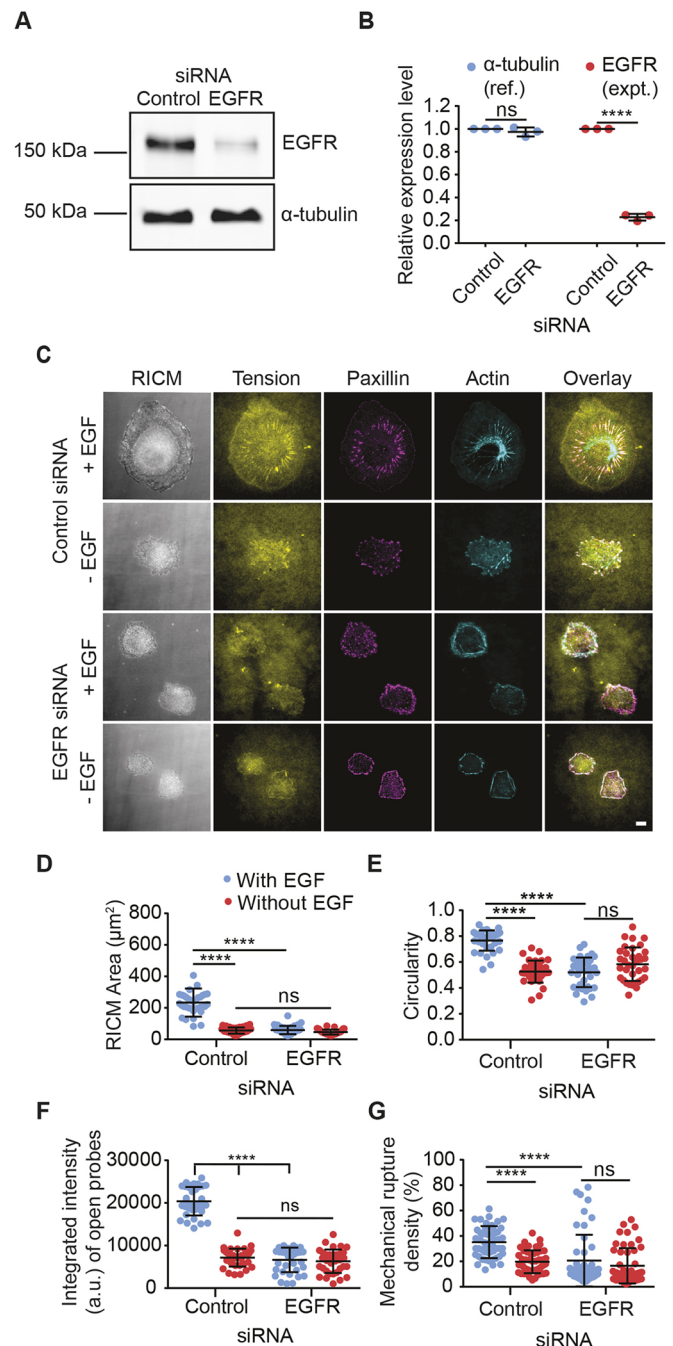


Fig. 6. EGFR silencing leads to reduced cell spreading and integrin tension.

(A) Western blot analysis of cell lysates from Cos-7 cells transfected with scrambled (control) or EGFR siRNA at 72 h after transfection and probed with anti-EGFR and anti- α -tubulin (reference) antibodies. (B) Quantification of the relative expression levels of EGFR and α -tubulin. EGFR siRNA transfection resulted in an 80% reduction in EGFR protein compared with control siRNA. (C) Cos-7 cells transfected with scrambled control or EGFR siRNA were dissociated and plated on 56 pN TGT surface in the presence or absence of EGF for 1 h. (D–G) Scatter plots representing the cell footprint: RICM spread area (D), cell circularity (E), integrated intensity of open probes (F) and the mechanical rupture density (G) for Cos-7 cells following siRNA-induced EGFR knockdown with or without EGF stimulation ($n=25$ cells, across three sets of experiments). Bars indicate mean \pm s.d. $^{ns}P>0.05$, $^{****}P<0.0001$ (one-way ANOVA). Scale bar: 10 μ m.

orientation despite EGF stimulation, similar to WT EGFR cells without stimulation (Fig. 7L). The EGFR penta mutant does not harbor the Src mutation, yet cell spreading and tension generation was

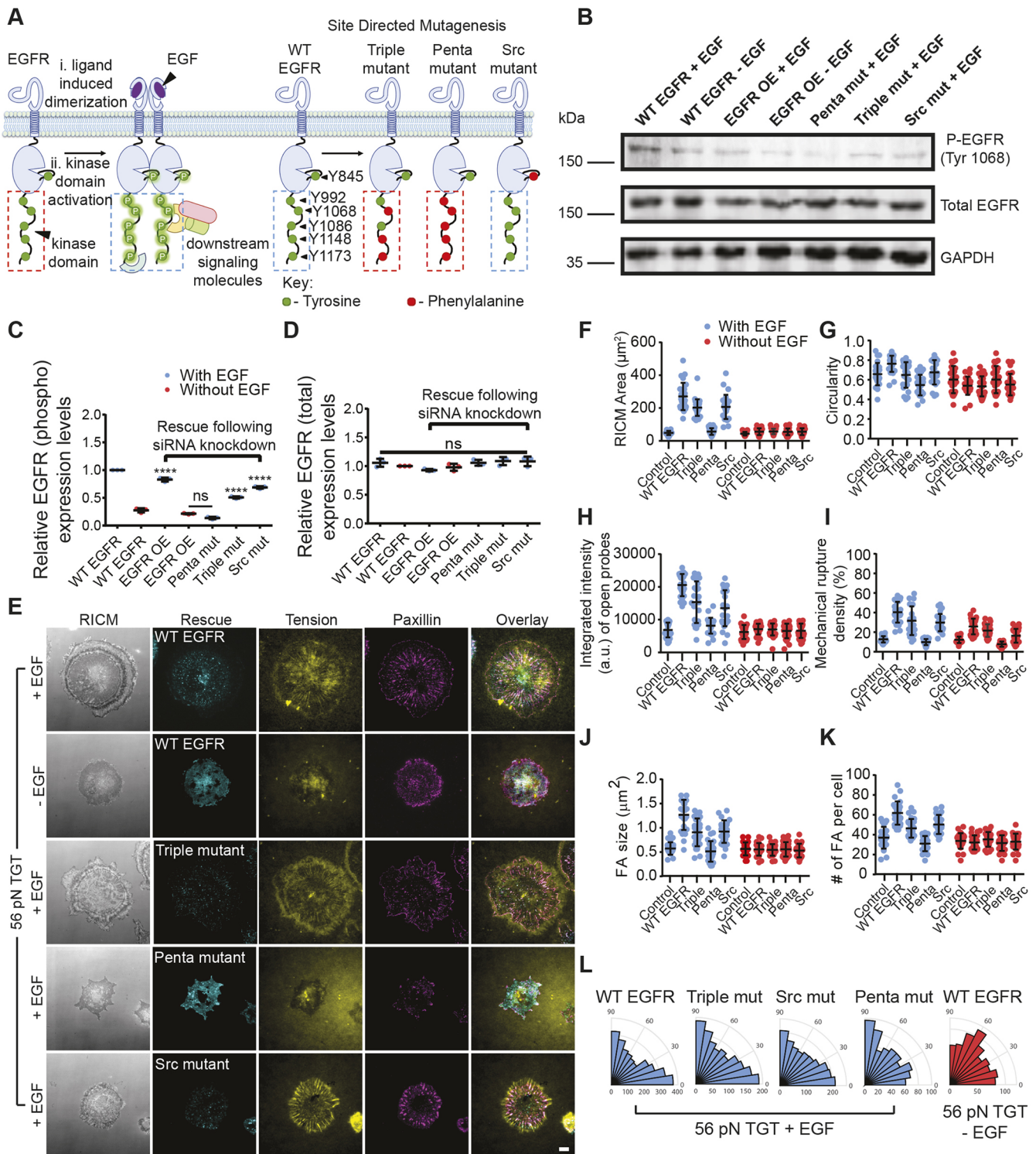


Fig. 7. Autophosphorylation of ligand-dependent EGFR kinase domain regulates cell spreading, integrin mechanics and FA organization. (A) Binding of EGF leads to conversion of the EGFR kinase domain from an inactive (green) to a catalytically active (fluorescent green) conformation characterized by receptor dimerization and recruitment of downstream signaling molecules (left). EGFR mutants created using site-directed mutagenesis (right). (B) Expression levels for the overexpressed EGFR variants were analyzed by western blot using lysates from EGFR-silenced Cos-7 cells rescued with the mutant or WT controls without silencing. (C,D) Semiquantitative analysis of EGFR activity: phospho-EGFR (C) and total EGFR (D) highlight the relative expression levels for the EGFR variants ($n=3$). (E) EGFR-silenced Cos-7 cells rescued via transfection with EGFP-tagged WT, triple, penta or Src kinase EGFR mutants. Cells were plated on a 56 pN TGT surface in presence or absence of EGF for 1 h and stained with paxillin. (F–K), Scatter plots representing the cell footprint: RICM spread area (F), cell circularity (G), integrated intensity of open probes (H), mechanical rupture density (I), FA size (J) and the number of FAs per cell (K) for Cos-7 cells following rescue with or without EGF stimulation. (L) Rose plots showing the distribution of radial angles marking FA orientation in the indicated cells (WT EGFR with EGF, $n=46$ cells; WT EGFR without EGF, $n=32$ cells; Src mutant and penta mutant with EGF, $n=25$ cells; triple mutant with EGF, $n=22$ cells; three independent experiments). Bars indicate mean \pm s.d. $^{ns}P>0.05$, $^{****}P<0.0001$ (one-way ANOVA). For F–K, P -values are not shown due to numerous comparisons; see Tables S1–S6 for detailed ANOVA data. Scale bar: 10 μm

completely abrogated, suggesting no rescue of these phenotypes by ligand-independent EGFR signaling. Our data show a central role for ligand-dependent EGFR activation in regulating cell spreading, mechanics and FA organization.

DISCUSSION

Our results show that activated EGFR directly regulates integrin mechanics, cell spreading, FA organization and maturation (Fig. 8A,B). The TGT surfaces provide a cumulative readout of integrin tension, or the force history of the cell (Ma and Salaita, 2019; Wang et al., 2018b). TGTs also allowed us to investigate the tension threshold for cell adhesion, which is not accessible with alternate approaches such as traction force or molecular tension fluorescence microscopy (Li et al., 2017). The simplicity of the TGT sensor design provided a minimal platform to study EGFR-integrin signaling crosstalk in isolation from other membrane receptors (Blanchard and Salaita, 2019). Although the TGT sensors uniquely allowed us to probe the tension threshold for cell adhesion, there are several nuances that should not be overlooked. First, the tension image does not represent real-time receptor-ligand interactions because fluorescence is generated following probe rupture. Thus, the fluorescent signal corresponds to probes that are no longer experiencing tension. Second, because TGT rupture effectively terminates the receptor-ligand interaction, the ability of cells to spread on a surface is reflected by ligand-receptor pairs experiencing forces less than T_{tol} . This artificial ‘slip-plane’, where the ligands (representing the matrix) are not well anchored, may elicit differences compared to a system where ligands are well anchored and linkages are maintained. Third, we employed TGTs with a single force threshold, T_{tol} , that is defined under ideal conditions as the constant force that has a 50% probability of rupturing the probe during an observation period of 2 s. In real biological systems, TGT probes can experience tension with complicated and heterogeneous time-dependencies. Therefore, the fluorescent signal of open probes does not directly report the magnitude of force under all conditions (Murad and Li, 2019; Yasunaga et al., 2019). For example, forces below T_{tol} applied for a long duration could rupture the same number of probes as a force above T_{tol} applied for a short duration. Each would result in the same fluorescence intensity (Yasunaga et al., 2019). Because we were unable to resolve exact tension magnitudes and dynamics using TGT probes, our results were interpreted with caution. For these reasons, our assessments of integrin tension were made by carefully designing experiments with internal controls, use of fibronectin-coated surfaces, comparative assessment of TGT fluorescence in cells with or without EGF stimulation, and use of TGTs with distinct rupture thresholds. We acknowledge the limitations of the mechanical rupture density measurement, because RICM reports the final spread area of the cell whereas the TGT signal represents an accumulated signal over the entire duration of cell spreading and adhesion. Thus, if a cell accelerated its spreading or migration, the apparent mechanical rupture density would appear weaker. Nonetheless, this parameter provides a powerful quantitative tool for better understanding of the role of EGF signaling in modulating integrin traction forces.

Together, the EGF and RGD ligands used here are the minimal essential signals required for regulation of early adhesion formation and cell spreading. We found that activated EGFR promotes and organizes integrin tension and lowers the tension threshold for cell spreading (Fig. 8B). EGF led to an increase in integrin tension, possibly by influencing the membrane distribution or force-loading properties of integrins. We posit

that EGFR acts as a ‘mechano-organizer’ based on its ability to enhance the spatial organization of tension and FAs and modulate the mechanics of force-bearing structures. Overall, our results show that ligand-dependent EGFR signaling promotes cell spreading, loading of integrins and FA maturation. One possible mechanism by which EGFR influences integrin tension and cell spreading is via reorganization of the actin cytoskeleton. We found that EGF promoted circularly arranged radial spokes of actin anchored at FAs in Cos-7 cells on both TGT surfaces. Overall, the combined increases in integrated tension, FA size and spread area could indicate active engagement of radial actin fibers at FA contact sites, a phenomenon previously reported (Jalal et al., 2019; Rape et al., 2011; Reinhart-King et al., 2005). We propose that activated EGFR could regulate the interaction of contractile transverse fibers containing myosin with radial actin filaments modulating force transmission to the FAs via integrins (Tee et al., 2015). Moreover, inhibition of Rac1 and RhoA blocked the effects of EGF, illustrating the role of these proteins downstream of EGFR in cell spreading and adhesion.

Myosin II motor proteins have a central role in generating cell forces, and it should be noted that Cos-7 cells express myosin IIB but not myosin IIA (Even-Ram et al., 2007). Myosin II isoforms have considerable sequence homology and can co-assemble into a single filament (Beach et al., 2014; Shutova et al., 2017). However, distinct mechanical roles for myosin IIA and IIB have been identified in lamellipodia extension, spreading and migration (Dasbiswas et al., 2018). During spreading, myosin IIB localizes at cell margins and drives lamellipodia extension by generating protrusive forces (Betapudi, 2010). Our results complement these claims and led us to hypothesize that EGF stimulation in Cos-7 cells promotes attachment and spreading on the TGT surfaces via myosin IIB-driven protrusive forces.

We found that EGFR activation modulates the tension threshold for outside-in integrin signaling. Activated EGFR enhances processes downstream of integrin mechanics, including FA assembly and maturation, on substrates with lower tension tolerances. In contrast to previous work proposing a universal tension threshold of 33–40 pN for integrin activation, we advocate a tension threshold that is ‘tunable’ by ligand-dependent EGFR activation (Fig. 8C). The ability of EGFR to attenuate the mechanical threshold for integrin activation provides a mechanism for facilitating cell attachment and spreading on softer substrates (Wang and Ha, 2013). We hypothesize that EGFR–integrin crosstalk could control FA protein recruitment and localization to sites of contact formation via protein phosphorylation, as previously reported, thereby facilitating FA formation and maturation (Gilmore and Burridge, 1996; Hamadi et al., 2005; Hanks et al., 1992).

Our findings advise against viewing EGFR and integrins in isolation, but instead as a joint-sensing apparatus comparable to a signaling rheostat. Interestingly, we observed similar EGF-dependent responses across cell types from multiple species and origins, suggesting that the signaling rheostat is universal. The variations across the different cell lines in integrated tension and cell spreading could be attributed to differing expression levels or distribution of EGFR and integrins or other factors that regulate cell sensitivity to the mechanical environment, opening avenues for future research.

Cells detect soluble growth factors such as EGF as well as biophysical information contained within the ECM, including the presence of specific integrin ligands and substrate rigidity. Cancers, for example, are not solely driven by signal dysregulations, but are also heavily influenced by the tumor microenvironment (Huang and Ingber, 2005). Since integrin–EGFR crosstalk activates multiple signaling pathways involved in

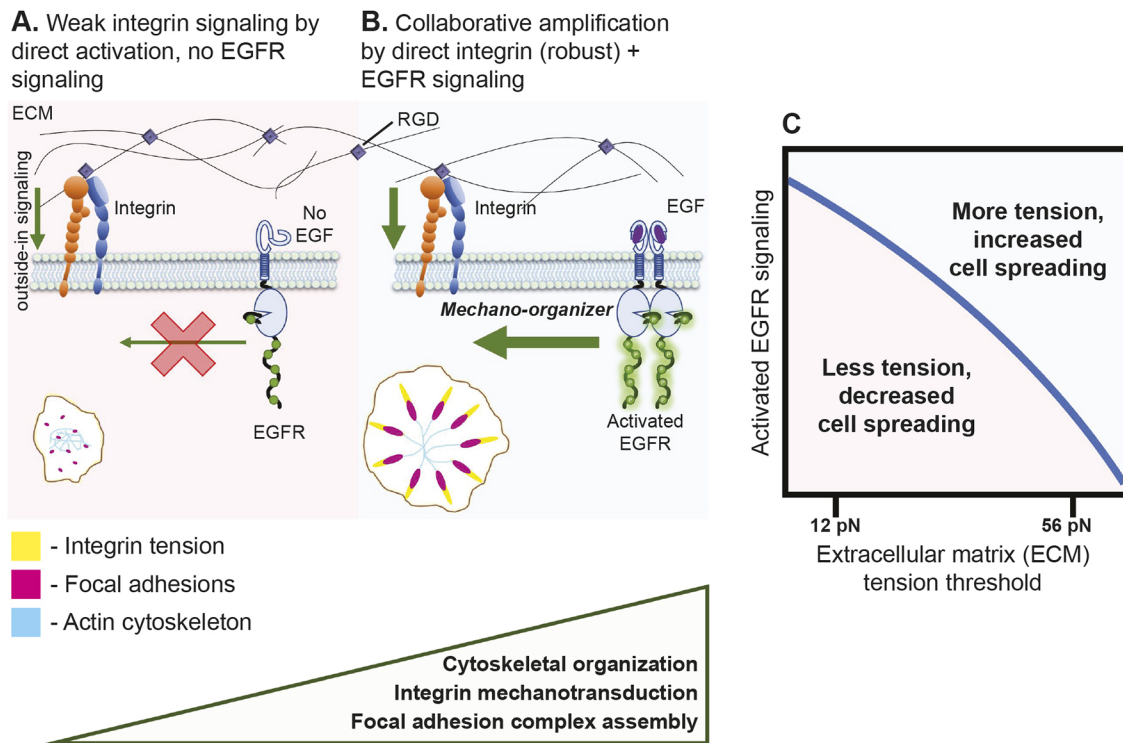


Fig. 8. EGFR promotes and organizes integrin mechanics. Model highlighting the role of EGFR signaling in cell spreading, FA organization and maturation, and integrin tension. (A) In the absence of EGF, integrin engagement of RGD results in low direct activation of the integrin signaling pathway. This results in formation of a limited number of immature FAs (magenta) with unorganized cytoskeleton (cyan), leading to relatively small cell spread areas and limited changes in cell morphology. (B) The lowered signaling from direct integrin activation can be rescued in the presence of EGF stimulation. Activated EGFR acts as a mechano-organizer, facilitating integrin tension (yellow), cytoskeletal rearrangement (cyan) and FA maturation (magenta). This results in cells with organized FAs and cytoskeleton, which enhances cell spreading. (C) The tension threshold of the underlying substrate plays an important role in integrin activation and regulation of FA formation and cell spreading (no EGF). However, this effect can be circumvented by activating the ligand-dependent EGFR signaling pathway, which in turn influences the cell mechanics (EGF). The blue trendline illustrates how the mechanical landscape responds to changes in EGF stimulation and tension threshold. EGF stimulation on both the 12 pN and 56 pN TGT surfaces results in collaborative amplification of the signaling pathways influencing cell mechanics. EGFR and integrin work together in a concerted manner, whereby activated EGFR attenuates (tunes) the integrin tension threshold for FA assembly, thus enhancing FA protein recruitment to sites of contact formation and resulting in formation of organized FAs on softer substrates. This 'mechano-organizing' property of EGFR regulates FA and cytoskeleton organization, resulting in increased cell spread area, irrespective of the TGT tension threshold.

cancer, our results suggest the possible impact of combinatorial therapies, targeting both integrin and EGFR, to combat tumors (Desgrosellier and Cheresh, 2010). Studying intermolecular-allosteric mechanisms involving EGFR, integrins and cell mechanics will further our understanding of cell behavior during complex processes such as adhesion, migration, differentiation, angiogenesis, tissue and organ development, invasion and metastasis. We posit that this allosteric regulation of cell mechanics is not limited to EGFR but is probably generalizable across the RTK family. Overall, our results bridge the gap between microenvironment sensing and intracellular signaling while highlighting a novel regulatory role for RTKs in regulating integrin mechanics.

MATERIALS AND METHODS

Synthesis of TGT strands

To prepare the cRGDfK-labeled TGT top strand, cyclo[Arg-Gly-Asp-D-Phe-Lys(PEG-PEG)] (Peptides International) peptide was coupled to NHS-azide (Thermo Fisher Scientific) as previously described (Zhang et al., 2014). cRGDfK-azide was coupled to the TGT top strand via a copper-assisted cycloaddition reaction. Briefly, cRGDfK-azide was mixed with the alkyne-21-BHQ2 oligonucleotide at a ratio of 2:1 (final concentrations ~200 μ M:100 μ M) in 100 μ l of 1 \times PBS containing 5 mM sodium ascorbate and 0.1 μ M preformed Cu-THPTA. The reaction was allowed to proceed at

room temperature (RT) for at least 4 h. The mixture was then subjected to P2 gel filtration to remove salts, organic solvent and unreacted reactants, and was further purified by reverse phase HPLC (solvent A was 0.1 M TEAA, solvent B was 100% MeCN; initial condition was 10% B with a gradient of 1%/min and flow rate of 1 ml/min).

The TGT bottom strands (12 pN or 56 pN) were coupled to Cy3B-NHS ester via nucleophilic substitution (Ma et al., 2016). In brief, the bottom TGT strand (either 12 pN or 56 pN, final concentration 100 μ M) was mixed with 50 μ g Cy3B-NHS ester (pre-dissolved in 10 μ l DMSO) in 0.1 M sodium bicarbonate solution (final volume 100 μ l, pH=9) and the reaction allowed to proceed overnight at RT. The mixture was then subjected to P2 gel filtration to remove salts, organic solvent and unreacted reactants, and was further purified by reverse-phase HPLC (conditions as above).

Oligonucleotide concentrations were determined by their absorbance at 260 nm using Nanodrop 2000 UV-Vis Spectrophotometer (Thermo Fisher Scientific). Both products were characterized by MALDI-TOF mass spectrometry performed on a high-performance Voyager STR (see Table S8). The MALDI matrix was freshly prepared by dissolving excess 3-hydroxyisobutyric acid into TA50 solvent (50:50 v/v acetonitrile and 0.1% TFA in ddH₂O).

TGT surface preparation

TGT surfaces were prepared as previously described (Liu et al., 2016; Ma et al., 2016). Briefly, #2 coverslips (25 mm, VWR) were sonicated for 10 min in 200 proof alcohol (Decon Labs) followed by cleaning in piranha solution (3:1 H₂SO₄ and H₂O₂, Thermo Fisher Scientific) for 30 min.

Coverslips were then washed six times with MilliQ water and twice with ethanol, bonded with 3% (v/v) APTES (Sigma) in ethanol for 1 h, washed three times with ethanol and dried using a stream of N₂ gas. Coverslips were then reacted with 2 mg/ml sulfo-NHS-biotin (Thermo Fisher Scientific) in DMSO (Thermo Fisher Scientific) and incubated overnight at 4°C. The next day, coverslips were washed three times with ethanol and dried with N₂. The surfaces were treated with 0.1% bovine serum albumin (Thermo Fisher Scientific) in 1× PBS to block any nonspecific sites. Following three washes with PBS, surfaces were treated with a solution of 1 µg/ml streptavidin (Thermo Fisher Scientific). After 45 min, the surfaces were washed three times with PBS and incubated for 1 h at RT with 100 µl of 50 nM pre-assembled DNA tension probes (for synthesis and validation see Tables S7, S8). The pre-assembly was carried out in a thermocycler by incubating the TGT probe mixture at 25°C for 25 min following an initial denaturation at 95°C for 5 min. The surfaces were finally washed three times with PBS and were ready for imaging. Just before imaging, surfaces were switched into Fluorobrite medium with or without EGF (Sigma), depending on the specific experiment, and the cells added. TGT surfaces were used within 24 h of synthesis.

Fibronectin surface preparation

Precleaned glass coverslips were coated at a final concentration of 10 µg/ml with a minimal volume of the diluted fibronectin in PBS. The surfaces were incubated for at least 45 min at room temperature before excess fibronectin was removed by aspiration and the surfaces dried for 3 h prior to the experiment. Just before imaging, slides were switched into Fluorobrite medium with or without EGF (Sigma), depending on the experimental requirement, before plating cells.

Cell culture and reagents

Cos-7 (African green monkey kidney fibroblast), NIH/3T3 (mouse embryo fibroblasts) and HeLa (human cervix epithelioid carcinoma) cells were cultured in Dulbecco's modified Eagle's medium (DMEM; Corning) containing L-glutamine and sodium pyruvate. ATDC5 (mouse teratocarcinoma) and OV4 (human ovarian adenocarcinoma) cells were cultured in medium comprising a 1:1 ratio of DMEM containing L-glutamine and sodium pyruvate and Ham's F-12K media (Corning). All media were supplemented with 10% fetal bovine serum (Life Technologies) and 100 IU/ml penicillin-streptomycin (Life Technologies). Cells were maintained at 37°C and 5% CO₂. When tested, the cells were found negative for mycoplasma contamination. Cells were imaged in Fluorobrite DMEM without any serum supplementation in the presence or absence of EGF (Sigma Aldrich). EGF was diluted (50 ng/ml) in Fluorobrite. Specific concentrations used for the pharmacological inhibitors diluted in DMSO were as follows: SB273005 (2.5 nM; Selleckchem), latrunculin B (4 µM; Sigma), blebbistatin (20 µM; Selleckchem), CCG-1423 (300 nM; Selleckchem), NSC 23766 (50 µM Selleckchem), erlotinib HCl (20 nM; Selleckchem), tyrphostin AG-1478 (30 nM; Selleckchem), PP2 (200 nM Selleckchem). The reagents and dilutions for staining were as follows: paxillin (1:250; Abcam, ab32084), phalloidin (1:400; Cell Signaling, 8878s), pEGFR Tyr1068 (1:800; Cell Signaling, 3777s) and AlexaFluor-647 labeled goat anti-rabbit secondary antibody (1:800; Invitrogen, A-21244).

Cell dissociation and stimulation

Cells growing on a culture dish were washed in Hank's balanced salt solution (Corning) and dissociated with trypsin (Sigma). Following detachment, residual trypsin was neutralized prior to plating cells on the TGT surfaces. Medium on the TGT surfaces was switched to Fluorobrite with or without EGF according to the experiment prior to cell addition. For the live cell experiments, the TGT surfaces were placed in a Tokai Hit incubation chamber at 37°C and 5% CO₂ prior to cell plating to minimize the time between plating and imaging. The medium was switched to Fluorobrite with or without EGF at the specified time point in an experiment-dependent manner. For inhibitor studies, cells were incubated in Fluorobrite supplemented with the indicated inhibitor for the entire incubation period.

Immunostaining

Cos-7 cells were allowed to spread on the TGT surface for 60 min at 37°C with 5% CO₂. After this, cells were fixed for 15 min in 4% (v/v)

formaldehyde (Electron Microscopy Sciences) in 1× PBS at 37°C in a shaker with mild agitation (35 rpm). Following five subsequent washes, cells were permeabilized and blocked for 30 min with 0.25% (v/v) Triton X-100 (Thermo Fisher Scientific) and 1% BSA. Cells were stained for the actin cytoskeleton using phalloidin, for FAs using paxillin antibody and for activated EGFR using the pEGFR antibody.

Microscopy

Cells were imaged with total internal reflection fluorescence (TIRF) and reflective interference contrast microscopy (RICM) on a Nikon Eclipse Ti2 microscope with Nikon Perfect Focus System driven by the Nikon Elements software package. Cells were imaged with an oil immersion Apo TIRF 60× NA 1.49 objective and a cooled electron-multiplying charge-coupled device camera (iXon3; Andor Technology). The sample was illuminated with a Sola epifluorescence light source (Lumencor) for RICM or with 405, 488, 561 or 638 nm lasers for TIRF. All live cell experiments were performed at 37°C with 5% CO₂ in a heated micro-incubator (Tokai Hit, Shizuoka-ken) and the fixed cell experiments at RT.

Site directed mutagenesis

The EGFP-tagged EGFR triple (Y1068F, Y1148F, Y1173F), penta (Y992F, Y1068F, Y1086F, Y1148F, Y1173F) and Src kinase (Y845F) mutants were generated using the Quikchange-II site-directed mutagenesis kit (Agilent) and the primers listed in Table S9. The mutations were made in the parent plasmid EGFR-GFP (Addgene #32751, deposited by Alexander Sorkin) (Carter and Sorkin, 1998). All constructs were sequenced to confirm the specific mutation(s).

EGFR silencing and rescue

Cos-7 cells were seeded into a six-well plate to reach 60-70% confluence on the day of transfection. At 24 h after seeding, cells were transfected with 25 µM of EGFR siRNA (pre-mix EGFR siRNA, Qiagen, SI00300104) or scrambled control siRNA (Qiagen, 1022076) using Lipofectamine RNAi MAX (Invitrogen). For rescue experiments, plasmids were transfected 72 h (day 3) after the initial silencing using Lipofectamine 3000 (Invitrogen) following the manufacturer's protocol. The transfected cells were imaged 48 h following rescue.

Western blot analysis

To validate EGFR expression following siRNA knockdown, protein was extracted by cell lysis 72 h after siRNA transfection and 25 µg of protein per sample was loaded into each well. To validate the EGFR expression levels following rescue, each well was loaded with 50 µg of protein per sample (either from controls or cells expressing an EGFR variant) that had been extracted by cell lysis 48 h after rescue of the EGFR knockdown with EGFR variants. For validating the constitutive ErbB receptor family expression, 50 µg of protein per sample, with or without EGF treatment, was loaded into each well following cell lysis. Primary antibodies were incubated overnight at 4°C. Antibodies included EGFR (D38B1) XP (1:1000; Cell Signaling, 4267s), phospho-EGFR (Tyr1068) (D7A5) XP (1:800; Cell Signaling, 3777), phospho-ErbB2 (Tyr1221/1222) (6B12) (1:1000; Cell Signaling, 2243), phospho-ErbB3 (Tyr1289) (D1B5) (1:1000; Cell Signaling, 2842), phospho-ErbB4 (Tyr1284) (21A9) (1:1000; Cell Signaling, 4757), α -tubulin mouse monoclonal antibody (1:2500; Developmental Studies Hybridoma Bank, 12G10) and GAPDH (D4C6R) (1:1000; Cell Signaling, 97166). Secondary antibodies were incubated for 30 min at RT. Antibodies included AlexaFluor 680-conjugated goat anti-rabbit IgG (1:10,000; Life Technologies, A21109), goat anti-mouse IgG (1:15,000; Li-Cor, 926-32210, IRDye 800CW), goat anti-rabbit IgG (1:15,000; Li-Cor, 925-32211, IRDye 800CW) and goat anti-mouse IgG (1:20,000; Li-Cor, 925-68020, IRDye 680LT). Images were captured with an Odyssey Image Station (Li-Cor) and the Odyssey Application Software (3.0, Li-Cor) was used for quantification of the band intensities.

Image processing and statistical analysis

Images were analysed using Fiji (ImageJ, National Institutes of Health, Bethesda, MD), Nikon Elements and MATLAB. For all images, the LUT

was normalized to the same threshold limits representing the full dynamic range. Image processing was performed with custom-written ImageJ macros to subtract background fluorescence and measure morphological parameters, including area of the cell footprint (RICM area), circularity and integrated tension. The cell footprint obtained from the RICM image was outlined manually to define the cell boundary for tension calculations. The integrated tension was determined by calculating the total TGT fluorescence intensity for the open probes within the cell boundary and subtracting the background measured from an off-cell region. The TGT background corresponds to the fluorescence from quenched TGT probes not experiencing any cellular tension. For live-cell time-lapse imaging, cell area changes were measured by comparing the RICM area at t min with the area at $t-10$ min. The change in cell area was normalized to the cell area at the first time point prior to addition of EGF for every individual cell.

Colocalization of paxillin and integrin tension was calculated with the Pearson's correlation coefficient using the JACoP (Just Another Colocalization Plugin) plugin in Fiji. FA size and number was quantified as previously described (Horzum et al., 2014). The radial angle of FAs was calculated using a custom MATLAB script (available on request), which first identified paxillin puncta and the RICM cell border. The algorithm selected cells with no overlap with neighboring cells. The geometrical centroid of each cell was used to calculate the radial angle, which is the minimum angle between axis 1 (an axis pointing through the cell centroid and the FA centroid) and axis 2 (the long axis of the focal adhesion). Each FA was treated as an independent sample for the analysis.

All results are presented as mean \pm s.d. unless otherwise noted. Statistical calculations were performed using Prism6 software (GraphPad). One-way ANOVA was used to quantify the statistical significance.

Acknowledgements

The authors would like to thank Dr Jeremy Herskowitz and Kelsey Greathouse for resources and expertise, and Reena R. Beggs for fruitful discussions and critiques.

Competing interests

The authors declare no competing or financial interests.

Author contributions

Conceptualization: T.C.R., K.S., A.L.M.; Methodology: T.C.R., V.P.-Y.M., S.G., K.S., A.L.M.; Software: A.B.; Formal analysis: T.C.R., V.P.-Y.M., A.B., T.M.U.; Investigation: T.C.R.; Resources: V.P.-Y.M., K.S., A.L.M.; Writing - original draft: T.C.R.; Writing - review & editing: T.C.R., V.P.-Y.M., A.B., T.M.U., K.S., A.L.M.; Visualization: T.C.R., A.L.M.; Supervision: A.L.M.; Project administration: T.C.R., A.L.M.; Funding acquisition: K.S., A.L.M.

Funding

This work was supported by funding to A.L.M. from the National Science Foundation (NSF) CAREER (1832100) and to A.L.M. and K.S. from the National Institutes of Health (NIH) (R01GM131099). Deposited in PMC for release after 12 months.

Supplementary information

Supplementary information available online at <https://jcs.biologists.org/lookup/doi/10.1242/jcs.238840.supplemental>

References

- Beach, J. R., Shao, L., Remmert, K., Li, D., Betzig, E. and Hammer, J. A. III. (2014). Nonmuscle myosin II isoforms coassemble in living cells. *Curr. Biol.* **24**, 1160-1166. doi:10.1016/j.cub.2014.03.071
- Betapudi, V. (2010). Myosin II motor proteins with different functions determine the fate of lamellipodia extension during cell spreading. *PLoS one* **5**, e8560. doi:10.1371/journal.pone.0008560
- Blanchard, A. T. and Salaita, K. (2019). Emerging uses of DNA mechanical devices. *Science* **365**, 1080-1081. doi:10.1126/science.aax3343
- Carter, R. E. and Sorkin, A. (1998). Endocytosis of functional epidermal growth factor receptor-green fluorescent protein chimera. *J. Biol. Chem.* **273**, 35000-35007. doi:10.1074/jbc.273.52.35000
- Chiasson-MacKenzie, C. and McClatchey, A. I. (2018). EGFR-induced cytoskeletal changes drive complex cell behaviors: the tip of the iceberg. *Sci. Signal.* **11**, eaas9473. doi:10.1126/scisignal.aas9473
- Choi, C. K., Vicente-Manzanares, M., Zareno, J., Whitmore, L. A., Mogilner, A. and Horwitz, A. R. (2008). Actin and α -actinin orchestrate the assembly and maturation of nascent adhesions in a myosin II motor-independent manner. *Nat. Cell Biol.* **10**, 1039-1050. doi:10.1038/ncb1763
- Chowdhury, F., Li, I. T. S., Leslie, B. J., Doğanay, S., Singh, R., Wang, X., Seong, J., Lee, S.-H., Park, S., Wang, N. et al. (2015). Single molecular force across single integrins dictates cell spreading. *Integr. Biol.* **7**, 1265-1271. doi:10.1039/C5IB00080G
- Dan, L., Jian, D., Na, L. and Xiaozhong, W. (2012). Crosstalk between EGFR and integrin affects invasion and proliferation of gastric cancer cell line, SGC7901. *Oncotargets Ther.* **5**, 271-277. doi:10.2147/OTT.S35322
- Dasbiswas, K., Hu, S., Schnorrer, F., Safran, S. A. and Bershadsky, A. D. (2018). Ordering of myosin II filaments driven by mechanical forces: experiments and theory. *Philos. Trans. R. Soc. Lond. B Biol. Sci.* **373**, 20170114. doi:10.1098/rstb.2017.0114
- Desgrosellier, J. S. and Cheresh, D. A. (2010). Integrins in cancer: biological implications and therapeutic opportunities. *Nat. Rev. Cancer* **10**, 9-22. doi:10.1038/nrc2748
- Duong, L. T. and Coleman, P. J. (2002). Ligands to the integrin receptor α v β 3. *Expert Opin. Ther. Patents* **12**, 1009-1021. doi:10.1517/13543776.12.7.1009
- Eberwein, P., Laird, D., Schulz, S., Reinhard, T., Steinberg, T. and Tomakidi, P. (2015). Modulation of focal adhesion constituents and their downstream events by EGF: on the cross-talk of integrins and growth factor receptors. *Biochim. Biophys. Acta* **1853**, 2183-2198. doi:10.1016/j.bbamcr.2015.06.004
- Evelyn, C. R., Wade, S. M., Wang, Q., Wu, M., Iñiguez-Lluhi, J. A., Merajver, S. D. and Neubig, R. R. (2007). CCG-1423: a small-molecule inhibitor of RhoA transcriptional signaling. *Mol. Cancer Ther.* **6**, 2249. doi:10.1158/1535-7163.MCT-06-0782
- Even-Ram, S., Doyle, A. D., Conti, M. A., Matsumoto, K., Adelstein, R. S. and Yamada, K. M. (2007). Myosin IIA regulates cell motility and actomyosin-microtubule crosstalk. *Nat. Cell Biol.* **9**, 299-309. doi:10.1038/ncb1540
- Gardel, M. L., Schneider, I. C., Aratyn-Schaus, Y. and Waterman, C. M. (2010). Mechanical integration of actin and adhesion dynamics in cell migration. *Annu. Rev. Cell Dev. Biol.* **26**, 315-333. doi:10.1146/annurev.cellbio.011209.122036
- Giancotti, F. G. and Tarone, G. (2003). Positional control of cell fate through joint integrin/receptor protein kinase signaling. *Annu. Rev. Cell Dev. Biol.* **19**, 173-206. doi:10.1146/annurev.cellbio.19.031103.133334
- Gilmore, A. P. and Burridge, K. (1996). Molecular mechanisms for focal adhesion assembly through regulation of protein-protein interactions. *Structure* **4**, 647-651. doi:10.1016/S0969-2126(96)00069-X
- Hamadi, A., Bouali, M., Dontenwill, M., Stoeckel, H., Takeda, K. and Rondé, P. (2005). Regulation of focal adhesion dynamics and disassembly by phosphorylation of FAK at tyrosine 397. *J. Cell Sci.* **118**, 4415-4425. doi:10.1242/jcs.02565
- Hanks, S. K., Calalb, M. B., Harper, M. C. and Patel, S. K. (1992). Focal adhesion protein-tyrosine kinase phosphorylated in response to cell attachment to fibronectin. *Proc. Natl. Acad. Sci. USA* **89**, 8487-8491. doi:10.1073/pnas.89.18.8487
- Helin, K. and Beguinot, L. (1991). Internalization and down-regulation of the human epidermal growth factor receptor are regulated by the carboxyl-terminal tyrosines. *J. Biol. Chem.* **266**, 8363-8368.
- Horzum, U., Ozdil, B. and Pesen-Okvur, D. (2014). Step-by-step quantitative analysis of focal adhesions. *MethodsX* **1**, 56-59. doi:10.1016/j.mex.2014.06.004
- Huang, S. and Ingber, D. E. (2005). Cell tension, matrix mechanics, and cancer development. *Cancer Cell* **8**, 175-176. doi:10.1016/j.ccr.2005.08.009
- Huveneers, S. and Danen, E. H. J. (2009). Adhesion signaling – crosstalk between integrins, Src and Rho. *J. Cell Sci.* **122**, 1059-1069. doi:10.1242/jcs.039446
- Iwabu, A., Smith, K., Allen, F. D., Lauffenburger, D. A. and Wells, A. (2004). Epidermal growth factor induces fibroblast contractility and motility via a protein kinase C δ -dependent pathway. *J. Biol. Chem.* **279**, 14551-14560. doi:10.1074/jbc.M311981200
- Jalal, S., Shi, S., Acharya, V., Huang, R. Y.-J., Viasnoff, V., Bershadsky, A. and Tee, Y. H. (2019). Actin cytoskeleton self-organization in single epithelial cells and fibroblasts under isotropic confinement. *J. Cell Sci.* **132**, jcs.220780. doi:10.1242/jcs.220780
- Kakiashvili, E., Dan, Q., Vandermeer, M., Zhang, J., Waheed, F., Pham, M. and Szasz, K. (2011). The epidermal growth factor receptor mediates tumor necrosis factor- α -induced activation of the ERK/GEF-H1/RhoA pathway in tubular epithelium. *J. Biol. Chem.* **286**, 9268-9279. doi:10.1074/jbc.M110.179903
- Kantlehner, M., Schaffner, P., Finsinger, D., Meyer, J., Jonczyk, A., Diefenbach, B., Nies, B., Hölzemann, G., Goodman, S. L. and Kessler, H. (2000). Surface coating with cyclic RGD peptides stimulates osteoblast adhesion and proliferation as well as bone formation. *Chembiochem* **1**, 107-114. doi:10.1002/1439-7633(20000818)1:2<107::AID-CBIC107>3.0.CO;2-4
- Kapp, T. G., Rechenmacher, F., Neubauer, S., Maltsev, O. V., Cavalcanti-Adam, E. A., Zarka, R., Reuning, U., Notni, J., Wester, H.-J., Mas-Moruno, C. et al. (2017). A comprehensive evaluation of the activity and selectivity profile of ligands for RGD-binding integrins. *Sci. Rep.* **7**, 39805. doi:10.1038/srep39805
- Kloth, M. T., Laughlin, K. K., Biscardi, J. S., Boerner, J. L., Parsons, S. J. and Silva, C. M. (2003). STAT5b, a Mediator of Synergism between c-Src and the Epidermal Growth Factor Receptor. *J. Biol. Chem.* **278**, 1671-1679. doi:10.1074/jbc.M207289200
- Kok, R. J., Schraa, A. J., Bos, E. J., Moorlag, H. E., Ásgeirsdóttir, S. A., Everts, M., Meijer, D. K. F. and Molema, G. (2002). Preparation and functional evaluation

- of RGD-modified proteins as $\alpha v \beta 3$ integrin directed therapeutics. *Bioconjug. Chem.* **13**, 128-135. doi:10.1021/bc015561+
- Levy, M., Krobert, K. A., Wittig, K., Voigt, N., Bermudez, M., Wolber, G., Dobrev, D., Levy, F. O. and Wieland, T.** (2013). NSC23766, a widely used inhibitor of Rac1 activation, additionally acts as a competitive antagonist at muscarinic acetylcholine receptors. *J. Pharmacol. Exp. Ther.* **347**, 69. doi:10.1124/jpet.113.207266
- Li, I. T. S., Ha, T. and Chemla, Y. R.** (2017). Mapping cell surface adhesion by rotation tracking and adhesion footprinting. *Sci. Rep.* **7**, 44502. doi:10.1038/srep44502
- Liu, Y., Blanchfield, L., Ma, V. P.-Y., Andargachew, R., Galior, K., Liu, Z., Evavold, B. and Salaita, K.** (2016). DNA-based nanoparticle tension sensors reveal that T-cell receptors transmit defined pN forces to their antigens for enhanced fidelity. *Proc. Natl Acad. Sci. USA* **113**, 5610-5615. doi:10.1073/pnas.1600163113
- Ma, V. P.-Y. and Salaita, K.** (2019). DNA nanotechnology as an emerging tool to study mechanotransduction in living systems. *Small* **15**, 1900961. doi:10.1002/sml.201900961
- Ma, V. P.-Y., Liu, Y., Yehl, K., Galior, K., Zhang, Y. and Salaita, K.** (2016). Mechanically induced catalytic amplification reaction for readout of receptor-mediated cellular forces. *Angewandte Chemie Int. Edn.* **55**, 5488-5492. doi:10.1002/anie.201600351
- Masuda, H.-T., Ishihara, S., Harada, I., Mizutani, T., Ishikawa, M., Kawabata, K. and Haga, H.** (2014). Coating extracellular matrix proteins on a (3-aminopropyl)triethoxysilane-treated glass substrate for improved cell culture. *BioTechniques* **56**, 172-179. doi:10.2144/000114156
- Moendarbary, E. and Harris, A. R.** (2014). Cell mechanics: principles, practices, and prospects. *Wiley Interdiscip. Rev. Syst. Biol. Med.* **6**, 371-388. doi:10.1002/wsbm.1275
- Moro, L., Venturino, M., Bozzo, C., Silengo, L., Altruda, F., Beguinot, L., Tarone, G. and Defilippi, P.** (1998). Integrins induce activation of EGF receptor: role in MAP kinase induction and adhesion-dependent cell survival. *EMBO J.* **17**, 6622-6632. doi:10.1093/emboj/17.22.6622
- Moro, L., Dolce, L., Cabodi, S., Bergatto, E., Erba, E. B., Smeriglio, M., Turco, E., Retta, S. F., Giuffrida, M. G., Venturino, M. et al.** (2002). Integrin-induced Epidermal Growth Factor (EGF) receptor activation requires c-Src and p130Cas and leads to phosphorylation of specific EGF receptor tyrosines. *J. Biol. Chem.* **277**, 9405-9414. doi:10.1074/jbc.M109101200
- Mosayebi, M., Louis, A. A., Doye, J. P. K. and Ouldrige, T. E.** (2015). Force-induced rupture of a DNA duplex: from fundamentals to force sensors. *ACS Nano* **9**, 11993-12003. doi:10.1021/acs.nano.5b04726
- Murad, Y. and Li, I. T. S.** (2019). Quantifying molecular forces with serially connected force sensors. *Biophys. J.* **116**, 1282-1291. doi:10.1016/j.bpj.2019.02.027
- Paszek, M. J., Zahir, N., Johnson, K. R., Lakins, J. N., Rozenberg, G. I., Gefen, A., Reinhart-King, C. A., Margulies, S. S., Dembo, M., Boettiger, D. et al.** (2005). Tensional homeostasis and the malignant phenotype. *Cancer Cell* **8**, 241-254. doi:10.1016/j.ccr.2005.08.010
- Plotnikov, S. V., Pasapera, A. M., Sabass, B. and Waterman, C. M.** (2012). Force fluctuations within focal adhesions mediate ECM-rigidity sensing to guide directed cell migration. *Cell* **151**, 1513-1527. doi:10.1016/j.cell.2012.11.034
- Rape, A. D., Guo, W.-H. and Wang, Y.-L.** (2011). The regulation of traction force in relation to cell shape and focal adhesions. *Biomaterials* **32**, 2043-2051. doi:10.1016/j.biomaterials.2010.11.044
- Regad, T.** (2015). Targeting RTK signaling pathways in cancer. *Cancers (Basel)* **7**, 1758-1784. doi:10.3390/cancers7030860
- Reinhart-King, C. A., Dembo, M. and Hammer, D. A.** (2005). The dynamics and mechanics of endothelial cell spreading. *Biophys. J.* **89**, 676-689. doi:10.1529/biophysj.104.054320
- Ricono, J. M., Huang, M., Barnes, L. A., Lau, S. K., Weis, S. M., Schlaepfer, D. D., Hanks, S. K. and Cheresch, D. A.** (2009). Specific cross-talk between epidermal growth factor receptor and integrin $\alpha v \beta 5$ promotes carcinoma cell invasion and metastasis. *Cancer Res.* **69**, 1383-1391. doi:10.1158/0008-5472.CAN-08-3612
- Sato, K.-I., Nagao, T., Iwasaki, T., Nishihira, Y. and Fukami, Y.** (2003). Src-dependent phosphorylation of the EGF receptor Tyr-845 mediates Stat-p21waf1 pathway in A431 cells. *Genes Cells* **8**, 995-1003. doi:10.1046/j.1356-9597.2003.00691.x
- Saxena, M., Liu, S., Yang, B., Hajal, C., Changede, R., Hu, J., Wolfenson, H., Hone, J. and Sheetz, M. P.** (2017). EGFR and HER2 activate rigidity sensing only on rigid matrices. *Nat. Mater.* **16**, 775-781. doi:10.1038/nmat4893
- Schneider, I. C., Hays, C. K. and Waterman, C. M.** (2009). Epidermal growth factor-induced contraction regulates paxillin phosphorylation to temporally separate traction generation from de-adhesion. *Mol. Biol. Cell* **20**, 3155-3167. doi:10.1091/mbc.e09-03-0219
- Schwartz, M. A. and Ginsberg, M. H.** (2002). Networks and crosstalk: integrin signalling spreads. *Nat. Cell Biol.* **4**, E65. doi:10.1038/ncb0402-e65
- Shutova, M. S., Asokan, S. B., Talwar, S., Assoian, R. K., Bear, J. E. and Svitkina, T. M.** (2017). Self-sorting of nonmuscle myosins IIA and IIB polarizes the cytoskeleton and modulates cell motility. *J. Cell Biol.* **216**, 2877-2889. doi:10.1083/jcb.201705167
- Sorkin, A., Helin, K., Waters, C. M., Carpenter, G. and Beguinot, L.** (1992). Multiple autophosphorylation sites of the epidermal growth factor receptor are essential for receptor kinase activity and internalization. Contrasting significance of tyrosine 992 in the native and truncated receptors. *J. Biol. Chem.* **267**, 8672-8678.
- Streuli, C. H. and Akhtar, N.** (2009). Signal co-operation between integrins and other receptor systems. *Biochem. J.* **418**, 491-506. doi:10.1042/BJ20081948
- Tee, Y. H., Shemesh, T., Thiagarajan, V., Hariadi, R. F., Anderson, K. L., Page, C., Volkmann, N., Hanein, D., Sivaramakrishnan, S., Kozlov, M. M. et al.** (2015). Cellular chirality arising from the self-organization of the actin cytoskeleton. *Nat. Cell Biol.* **17**, 445. doi:10.1038/ncb3137
- Tong, J., Li, L., Ballermann, B. and Wang, Z.** (2016). Phosphorylation and activation of RhoA by ERK in response to epidermal growth factor stimulation. *PLoS ONE* **11**, e0147103. doi:10.1371/journal.pone.0147103
- Vasudevan, H. N. and Soriano, P.** (2016). Chapter Twenty-Three - a thousand and one receptor tyrosine kinases: wherein the specificity? *Curr. Top. Dev. Biol.* **117**, 393-404. doi:10.1016/bs.ctdb.2015.10.016
- Wang, X. and Ha, T.** (2013). Defining single molecular forces required to activate integrin and notch signaling. *Science* **340**, 991-994. doi:10.1126/science.1231041
- Wang, X., Sun, J., Xu, Q., Chowdhury, F., Roein-Peikar, M., Wang, Y. and Ha, T.** (2015). Integrin molecular tension within motile focal adhesions. *Biophys. J.* **109**, 2259-2267. doi:10.1016/j.bpj.2015.10.029
- Wang, X., Rahil, Z., Li, I. T. S., Chowdhury, F., Leckband, D. E., Chemla, Y. R. and Ha, T.** (2016). Constructing modular and universal single molecule tension sensor using protein G to study mechano-sensitive receptors. *Sci. Rep.* **6**, 21584. doi:10.1038/srep21584
- Wang, X., Zhang, L., Qu, R., Zhang, L. and Huang, W.** (2018a). Rho A regulates epidermal growth factor-induced human osteosarcoma MG63 cell migration. *Int. J. Mol. Sci.* **19**, 1437. doi:10.3390/ijms19051437
- Wang, Y., LeVine, D. N., Gannon, M., Zhao, Y., Sarkar, A., Hoch, B. and Wang, X.** (2018b). Force-activatable biosensor enables single platelet force mapping directly by fluorescence imaging. *Biosens. Bioelectron.* **100**, 192-200. doi:10.1016/j.bios.2017.09.007
- Wozniak, M. A., Modzelewska, K., Kwong, L. and Keely, P. J.** (2004). Focal adhesion regulation of cell behavior. *Biochim. Biophys. Acta Mol. Cell Res.* **1692**, 103-119. doi:10.1016/j.bbamcr.2004.04.007
- Xie, H., Paller, M. A., Gupta, K., Chang, P., Ware, M. F., Witke, W., Kwiatkowski, D. J., Lauffenburger, D. A., Murphy-Ullrich, J. E. and Wells, A.** (1998). EGF receptor regulation of cell motility: EGF induces disassembly of focal adhesions independently of the motility-associated PLCgamma signaling pathway. *J. Cell Sci.* **111**, 615-624.
- Yasunaga, A., Murad, Y. and Li, I. T. S.** (2019). Quantifying molecular tension—classifications, interpretations and limitations of force sensors. *Phys. Biol.* **17**, 011001. doi:10.1088/1478-3975/ab38ff
- Zhang, Y., Ge, C., Zhu, C. and Salaita, K.** (2014). DNA-based digital tension probes reveal integrin forces during early cell adhesion. *Nat. Commun.* **5**, 5167. doi:10.1038/ncomms6167
- Zhang, Y., Qiu, Y., Blanchard, A. T., Chang, Y., Brockman, J. M., Ma, V. P.-Y., Lam, W. A. and Salaita, K.** (2018). Platelet integrins exhibit anisotropic mechanosensing and harness piconewton forces to mediate platelet aggregation. *Proc. Natl Acad. Sci. USA* **115**, 325-330. doi:10.1073/pnas.1710828115